Recognition of the antigen-presenting molecule MR1 by a Vδ3$^+$ γδ T cell receptor

Michael T. Rice[a,b,c], Anouk von Borstel[a,b], Priyanka Chevour[a,b], Wael Awad[a,b], Lauren J. Howson[a,b,1], Dene R. Littler[a,b], Nicholas A. Gherardin[d,e], Jérôme Le Nours[a,b,c], Edward M. Giles[f,g], Richard Berry[a,b,c], Dale I. Godfrey[d,e], Martin S. Davey[a,b,c,2,3], Jamie Rossjohn[a,b,c,h,2,3], and Benjamin S. Gully[a,b,c,2,3]

[a]Infection and Immunity Program, Biomedicine Discovery Institute, Monash University, Clayton, VIC 3800, Australia; [b]Department of Biochemistry and Molecular Biology, Biomedicine Discovery Institute, Monash University, Clayton, VIC 3800, Australia; [c]Australian Research Council Centre of Excellence in Advanced Molecular Imaging, Monash University, Clayton, VIC 3800, Australia; [d]Department of Microbiology and Immunology, Peter Doherty Institute for Infection and Immunity, University of Melbourne, Melbourne, VIC 3000, Australia; [e]Australian Research Council Centre of Excellence in Advanced Molecular Imaging, University of Melbourne, Melbourne, VIC 3010, Australia; [f]Department of Paediatrics, Monash University, Clayton, VIC 3168, Australia; [g]Centre for Innate Immunity and Infectious Disease, Hudson Institute of Medicine, Clayton, VIC 3168, Australia; and [h]Institute of Infection and Immunity, Cardiff University School of Medicine, Cardiff CF14 4XN, UK

Edited by K. Christopher Garcia, Stanford University, Stanford, CA, and approved October 22, 2021 (received for review June 3, 2021)

Unlike conventional αβ T cells, γδ T cells typically recognize non-peptide ligands independently of major histocompatibility complex (MHC) restriction. Accordingly, the γδ T cell receptor (TCR) can potentially recognize a wide array of ligands; however, few ligands have been described to date. While there is a growing appreciation of the molecular bases underpinning variable (V)δ1$^+$ and Vδ2$^+$ γδ TCR-mediated ligand recognition, the mode of Vδ3$^+$ TCR ligand engagement is unknown. MHC class I–related protein, MR1, presents vitamin B metabolites to αβ T cells known as mucosal-associated invariant T cells, diverse MR1-restricted T cells, and a subset of human γδ T cells. Here, we identify Vδ1/2$^-$ γδ T cells in the blood and duodenal biopsy specimens of children that showed metabolite-independent binding of MR1 tetramers. Characterization of one Vδ3Vγ8 TCR clone showed MR1 reactivity was independent of the presented antigen. Determination of two Vδ3Vγ8 TCR-MR1-antigen complex structures revealed a recognition mechanism by the Vδ3 TCR chain that mediated specific contacts to the side of the MR1 antigen-binding groove, representing a previously uncharacterized MR1 docking topology. The binding of the Vδ3$^+$ TCR to MR1 did not involve contacts with the presented antigen, providing a basis for understanding its inherent MR1 autoreactivity. We provide molecular insight into antigen-independent recognition of MR1 by a Vδ3$^+$ γδ TCR that strengthens an emerging paradigm of antibody-like ligand engagement by γδ TCRs.

γδTCR | MR1 | structural immunology

Characterized by both innate and adaptive immune cell functions, γδ T cells are an unconventional T cell subset. While the functional role of γδ T cells is yet to be fully established, they can play a central role in antimicrobial immunity (1), antitumor immunity (2), tissue homeostasis, and mucosal immunity (3). Owing to a lack of clarity on activating ligands and phenotypic markers, γδ T cells are often delineated into subsets based on the expression of T cell receptor (TCR) variable (V) δ gene usage, grouped as Vδ2$^+$ or Vδ2$^-$.

The most abundant peripheral blood γδ T cell subset is an innate-like Vδ2$^+$subset that comprises ∼1 to 10% of circulating T cells (4). These cells generally express a Vγ9 chain with a focused repertoire in fetal peripheral blood (5) that diversifies through neonatal and adult life following microbial challenge (6, 7). Indeed, these Vγ9/Vδ2$^+$ T cells play a central role in antimicrobial immune response to *Mycobacterium tuberculosis* (8) and *Plasmodium falciparum* (9). Vγ9/Vδ2$^+$ T cells are reactive to prenyl pyrophosphates that include isopentenyl pyrophosphate and (E)-4-Hydroxy-3-methyl-but-2-enyl pyrophosphate (8) in a butyrophilin 3A1- and BTN2A1-dependent manner (10–13). Alongside the innate-like protection of Vγ9/Vδ2$^+$ cells, a Vγ9$^-$ population provides adaptive-like immunobiology with clonal expansions that exhibit effector function (14).

The Vδ2$^-$ population encompasses the remaining γδ T cells but most notably the Vδ1$^+$ and Vδ3$^+$ populations. Vδ1$^+$ γδ T cells are an abundant neonatal lineage that persists as the predominating subset in adult peripheral tissue including the gut and skin (15–18). Vδ1$^+$ γδ T cells display potent cytokine production and respond to virally infected and cancerous cells (19). Vδ1$^+$ T cells were recently shown to compose a private repertoire that diversifies, from being unfocused to a selected clonal TCR pool upon antigen exposure (20–23). Here, the identification of both Vδ1$^+$ T_{naive} and Vδ1$^+$ $T_{effector}$ subsets and the Vδ1$^+$ T_{naive} to $T_{effector}$ differentiation following in vivo infection point toward an adaptive phenotype (22).

The role of Vδ3$^+$ γδ T cells has remained unclear, with a poor understanding of their lineage and functional role. Early insights into Vδ3$^+$ γδ T cell immunobiology found infiltration of Vδ3$^+$ intraepithelial lymphocytes (IEL) within the gut mucosa of celiac patients (24). More recently it was shown that although Vδ3$^+$ γδ T cells represent a prominent γδ T cell

Significance

Alongside αβ T cells and B cells, γδ T cells comprise a major component of the adaptive immune system, although a lack of bona fide ligands has hindered understanding of their function. γδ T cells are key mediators of epithelial immune surveillance and have a purported capacity for employing diverse ligand engagement mechanisms beyond the dogmas of conventional αβ T cell–human leukocyte antigen restriction. Here, we found blood- and gut-resident Vδ1/2$^-$ γδ T cells bound to MR1 tetramers in a metabolite-independent mechanism distinct from mucosal-associated invariant T cells and provide insight into a unique antibody-like MR1 recognition mode. This reshapes our understanding of the ligand recognition principles of γδ T cells and how they differ from αβ T cells.

Author contributions: R.B., D.I.G., M.S.D., J.R., and B.S.G. designed research; M.T.R., A.v.B., P.C., W.A., L.J.H., D.R.L., and B.S.G. performed research; N.A.G., E.M.G., D.I.G., and M.S.D. contributed new reagents/analytic tools; M.T.R., A.v.B., L.J.H., J.L.N., M.S.D., J.R., and B.S.G. analyzed data; and M.T.R., M.S.D., J.R., and B.S.G. wrote the paper.

Competing interest statement: J.R. is an inventor on patents describing MR1 tetramers and MR1 ligands.

This article is a PNAS Direct Submission.

[1]Present address: Immunology Division, Walter and Eliza Hall Institute of Medical Research, Parkville, VIC 3052, Australia.

[2]M.S.D., J.R., and B.S.G. contributed equally to this work.

[3]To whom correspondence may be addressed. Email: martin.davey@monash.edu, jamie.rossjohn@monash.edu, or ben.gully@monash.edu.

This article contains supporting information online at http://www.pnas.org/lookup/suppl/doi:10.1073/pnas.2110288118/-/DCSupplemental.

Published November 29, 2021.

component of the gut epithelia and lamina propria in control donors, notwithstanding pediatric epithelium, the expanding population of T cells in celiac disease were Vδ1$^+$ (25). Although Vδ3$^+$ IELs compose a notable population of gut epithelia and lamina propria T cells (~3 to 7%), they also formed a discrete population (~0.2%) of CD4$^-$CD8$^-$ T cells in peripheral blood (26). These Vδ3$^+$ DN γδ T cells are postulated to be innate-like due to the expression of NKG2D, CD56, and CD161 (26). When expanded in vitro, these cells degranulated and killed cells expressing CD1d and displayed a T helper (Th) 1, Th2, and Th17 response in addition to promoting dendritic cell maturation (26). Peripheral Vδ3$^+$ γδ T cells frequencies are known to increase in systemic lupus erythematosus patients (27, 28), and upon cytomegalovirus (29) and HIV infection (30), although, our knowledge of their exact role and ligands they recognize remains incomplete.

The governing paradigms of antigen reactivity, activation principles, and functional roles of γδ T cells remain unresolved. This is owing partly due to a lack of knowledge of bona fide γδ T cell ligands. Presently, Vδ1$^+$ γδ T cells remain the best characterized subset with antigens including Major Histocompatibility Complex (MHC)-I (31), monomorphic MHC-I–like molecules such as CD1b (32), CD1c (33), CD1d (34), and MR1 (35), as well as more diverse antigens such as endothelial protein coupled receptor (EPCR) and phycoerythrin (PE) (36, 37). The molecular determinants of this reactivity were first established for Vδ1$^+$ TCRs in complex with CD1d presenting sulfatide (38) and α-galactosylceramide (α-GalCer) (34), which showed an antigen-dependent central focus on the presented lipids and docked over the antigen-binding cleft.

In humans, mucosal-associated invariant T (MAIT) cells are an abundant innate-like αβ T cell subset typically characterized by a restricted TCR repertoire (39–43) and reactivity to the monomorphic molecule MR1 presenting vitamin B precursors and drug-like molecules of bacterial origin (41, 44–46). Recently, populations of atypical MR1-restricted T cells have been identified in mice and humans that utilize a more diverse TCR repertoire for MR1-recognition (42, 47, 48). Furthermore, MR1-restricted γδ T cells were identified in blood and tissues including Vδ1$^+$, Vδ3$^+$, and Vδ5$^+$ clones (35). As seen with TRAV 1-2$^-$, unconventional MAITs cells the isolated γδ T cells exhibited MR1-autoreactivity with some capacity for antigen discrimination within the responding compartment (35, 48). Structural insight into one such MR1-reactive Vδ1$^+$ γδ TCR showed a down-under TCR engagement of MR1 in a manner that is thought to represent a subpopulation of MR1-reactive Vδ1$^+$ T cells (35). However, biochemical evidence suggested other MR1-reactive γδ T cell clones would likely employ further unusual docking topologies for MR1 recognition (35).

Here, we expanded our understanding of a discrete population of human Vδ3$^+$ γδ T cells that display reactivity to MR1. We provide a molecular basis for this Vδ3$^+$ γδ T cell reactivity and reveal a side-on docking for MR1 that is distinct from the previously determined Vδ1$^+$ γδ TCR-MR1-Ag complex. A Vδ3$^+$ γδ TCR does not form contacts with the bound MR1 antigen, and we highlight the importance of non–germ-line Vδ3 residues in driving this MR1 restriction. Accordingly, we have provided key insights into the ability of human γδ TCRs to recognize MR1 in an antigen-independent manner by contrasting mechanisms.

Results

Identification of an MR1 Responsive Population of Vδ3$^+$ γδ T cells. γδ T cells that exhibited MR1 autoreactivity, as well as a capacity for differential ligand recognition, were recently identified (35). These MR1-restricted γδ T cells were clonally diverse compared with the more restricted MAIT cell repertoire and represented ~0.001 to 0.1% of T cells in peripheral blood (35). The MR1-reactive γδ T cells contained a population of rare Vδ3$^+$ γδ TCRs (~28% of the sequenced clones). These cells were clonally diverse with no clonal focusing or CDR3 motifs present, a virtue thought to enable the Vδ1$^+$ compartment to adopt diverse recognition mechanisms for MR1. Here, we set out to characterize the molecular basis for Vδ3$^+$ γδ TCR recognition of MR1 (35).

Due to a lack of available reagents to directly identify Vδ3$^+$ γδ T cells, we first characterized γδ T cells in the peripheral blood and matched duodenal biopsies from children and young adults undergoing screening for celiac or inflammatory bowel disease (IBD) (aged between 1 to 17 y old; *SI Appendix*, Table S1). In a cohort of nine donors, with no intestinal disease, Vδ2$^+$ γδ T cells were the major subset (mean 58.1 ± 9.0%), followed by Vδ1$^+$ cells (mean 32.8 ± 7.8%), and then Vδ1/2$^-$ cells (mean 8.5 ± 2.0%) of peripheral γδ T cells (containing Vδ3$^+$, Vδ4$^+$, Vδ5$^+$, and Vδ8$^+$ γδ T cells) (Fig. 1*A*). In donor-matched duodenal biopsies, Vδ1$^+$ (56.3 ± 7.6%) and Vδ1/2$^-$ (mean 30.6 ± 7.4%) γδ T cells were enriched within γδ T cell populations (Fig. 1*A*), consistent with previous findings (24). All duodenum γδ T cell subsets expressed tissue-associated lymphocyte markers CD69 and CD103 (Fig. 1*B*).

We next performed a TCR repertoire analysis on the Vδ2$^-$ γδ T cell subsets from the blood and duodenum of two age-matched donors. The TCRδ-chain repertoires were highly enriched for Vδ1$^+$ TCR sequences in the blood and a few Vδ3$^+$ γδ TCR sequences (Fig. 1*C*). In the duodenum, Vδ1 and Vδ3 sequences were more equal in frequency. The TCRδ variable domains encoded within the alpha locus, namely Vδ4$^+$, Vδ5$^+$, Vδ6$^+$, Vδ7$^+$, and Vδ8$^+$, were scarce throughout blood and duodenum (Fig. 1*C*). Both blood and duodenum TCRδ sequences utilized Jδ1 regions (Fig. 1*C*). We also noted the presence of blood and duodenal Vδ2$^+$ TCR sequences within our sorted populations, likely due to a recently described Vγ9$^-$/Vδ2$^+$ γδ T cell subset that are also enriched in the liver tissue (14). Together, these data indicate that blood and duodenal Vδ1/2$^-$ cells are composed of Vδ3$^+$ γδ TCR sequences. There was a broad representation of all potential Vγ chain usage without any enrichment and use of Jγ2 or JγP2 in both blood and duodenum (Fig. 1*D*). Next, we assessed the clonotype diversity within the Vδ2$^-$ TCR repertoires in blood and duodenum. Tree plot (Fig. 1*E*), clonotype frequency (Fig. 1 *F*, *Top*), and diversity index (Fig. 1 *F*, *Bottom*) analysis indicated that the blood showed evidence of some expanded clonotypes and lower diversity than the matched duodenum. This diversity persisted despite the differing disease status of the donors. These data indicate that within the Vδ2$^-$ γδ T cell populations in blood and duodenum there are diverse clonotype repertoires.

Next, we conducted MR1 tetramer staining on matched blood and duodenal biopsies from five donors (aged 6 to 13; *SI Appendix*, Table S1), with three donors defined as normal and two donors with confirmed ulcerative colitis inflammation of the large intestine. Duodenal samples from ulcerative colitis patients are noninvolved tissue and showed no signs of disease-associated inflammation. In Vδ2$^-$ γδ T cells, we found varying degrees of both Vδ1$^+$ and Vδ1/2$^-$ MR1-tetramer$^+$ γδ T cells in both blood and duodenum. While we found Vδ1$^+$ T cells staining with MR1 tetramers, as we previously defined in the blood and duodenum (35), we now also identify Vδ1/2$^-$ γδ T cells staining with MR1 tetramers (Fig. 1*G*). Furthermore, Vδ1/2$^-$ MR1-tetramer$^+$ γδ T cells were detected across the cohort in normal and IBD donors, these cells tended to be more frequent in the blood of normal donors although larger studies at sites of IBD-associated inflammation in the terminal ileum and rectum are required to understand a potential role for these γδ T cells in disease. Moreover, MR1-tetramer$^+$ Vδ1/2$^-$ γδ T cells stained with both 5-OP-RU- and 6-FP–loaded MR1 tetramers

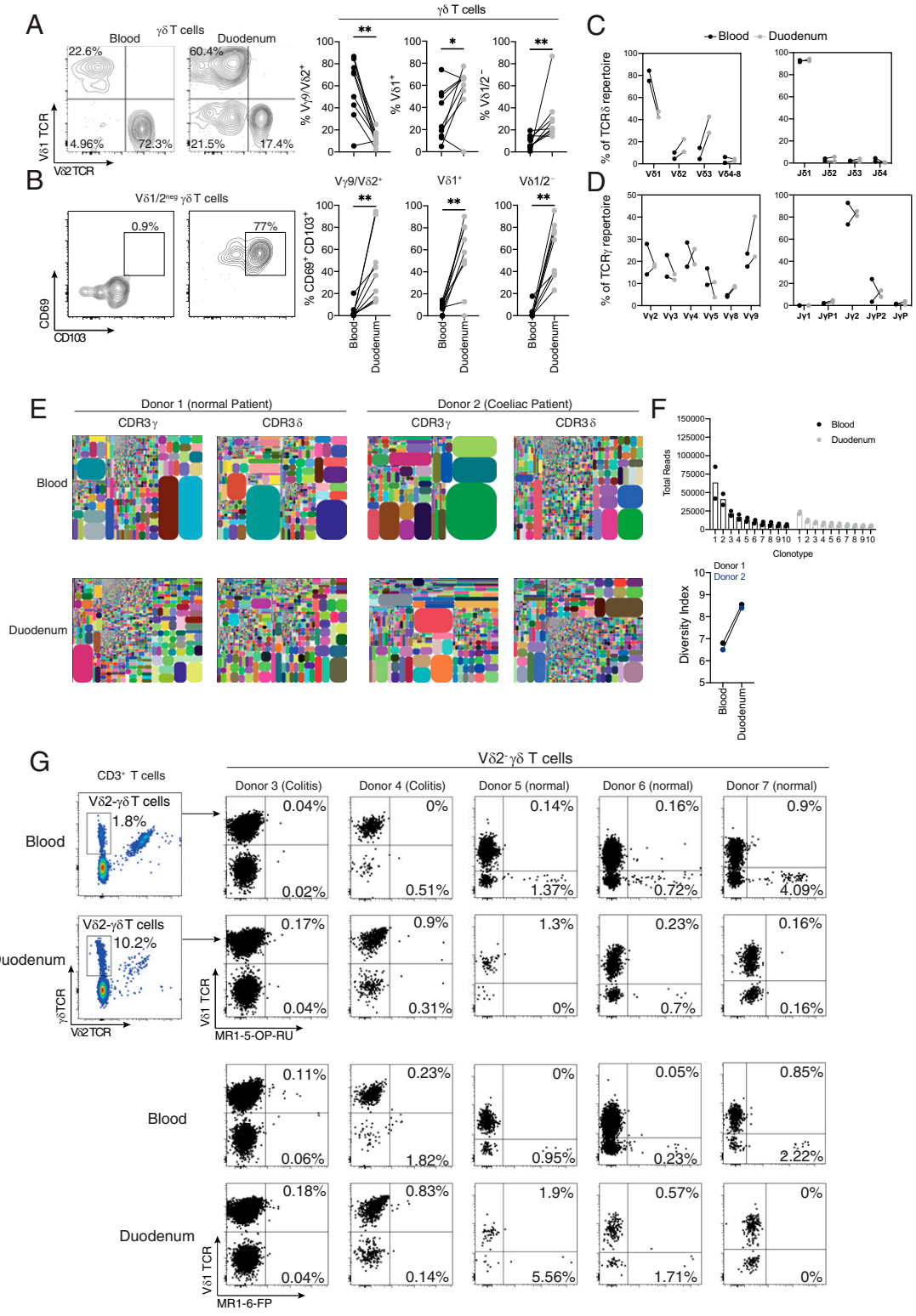

Fig. 1. Characterization of the γδ T cell repertoire and MR1-tetramer reactivity in matched blood and duodenum. Flow cytometry plots and graphs show matched human blood and duodenum (*A*) γδ T cell subset frequencies with total γδ T cells and (*B*) frequency of $CD69^+$ $CD103^+$ cells within each γδ T cell subset ($n = 9$). (*C*) Vδ and Jδ and (*D*) Vγ and Jγ usage in matched blood and duodenum sorted $Vδ2^-$ γδ T cells ($n = 2$). (*E*) Tree plots show CDR3γ and CDR3δ clonotype repertoires within sorted $Vδ2^-$ γδ T cells in peripheral blood and duodenum. Each color indicates a single CDR3 region, and the size indicates the number of reads for each clonotype. Colors do not match between tree plots. (*F*) Total reads for the top 10 CDR3 clonotypes (average of CDR3γ and δ shown) in matched blood and duodenum (*Top*) and average of CDR3γ and δ diversity index values; this metric considers the clonal frequency to occupy 50% of the total repertoire (D50) and abundance of unique CDR3 sequences (Shannon entropy) (*Bottom*) ($n = 2$). (*G*) Flow cytometry plots show $Vδ2^-$ γδ T cells from matched blood and duodenum stained with MR1-5-OP-RU or MR1-6FP tetramers ($n = 5$). All samples were stained with APC-MR1 tetramers, except Donor 7 duodenal samples were stained with BV421-MR1 tetramers. Lines indicate paired data. Normality was tested using the Shapiro–Wilk test; $*P < 0.05$; $**P < 0.01$; *P* values were determined by Wilcoxon matched-pairs signed rank test (*A* and *B*).

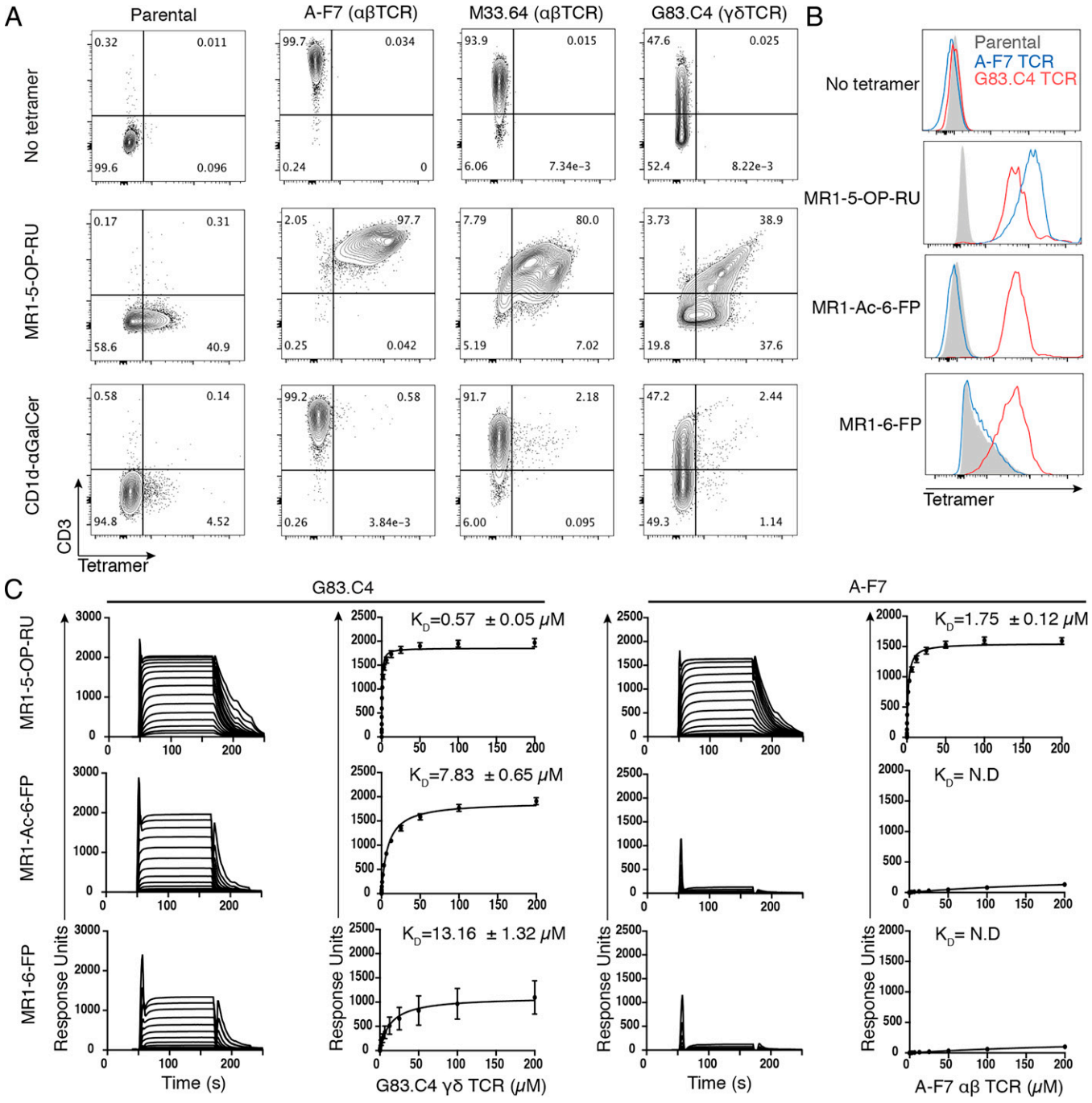

Fig. 2. Characterization of an MR1-reactive Vδ3+ γδ T cell clone G83.C4. (*A*) Flow cytometry plots showing antigen sensitivity of MR1 and CD1d-tetramer staining, of A-F7, M33.64 αβ MAIT TCRs, and Vδ3-Vγ8 G83.C4 γδ TCR-transduced Jurkat cells. (*B*) Histograms showing MR1-5-OP-RU, MR1-Ac-6-FP, and MR1-6-FP-tetramer reactivity of G83.C4 γδ and A-F7 αβ MAIT TCRs. (*C*) SPR binding affinity measurements of soluble G83.C4 γδ TCR and A-F7 αβ MAIT TCR for MR1-5-OP-RU, MR1-Ac-6-FP, and MR1-6-FP. Shown as binding affinity curves from a single dilution series experiment. Error bars denote SD from two repeat experiments performed in duplicate. N.D. = Not Determined.

(Fig. 1*G*), suggesting the potential for ligand-independent MR1 autoreactivity. Importantly, the blood MAIT cell population, defined by staining with the MR1-5-OP-RU tetramer, exhibited diminished responses to MR1-6-FP tetramers, recapitulating the well-defined antigen specificity of MAIT cells in these samples (*SI Appendix*, Fig. S1) (39–43, 47, 48). Hence, we allude to the identification of MR1-tetramer$^+$ populations of Vδ3$^+$ γδ T cells in clonally diverse γδ TCR repertoires found in blood and duodenum of children and young adults.

Vδ3 γδ TCR MR1 Antigen Reactivity and Specificity. We next set out to gain insight into the mediators of MR1 reactivity by Vδ3$^+$ γδ TCRs exemplified by the previously identified Vδ3-Vγ8 TCR clone termed G83.C4 for further analysis, as it became readily activated in response to MR1$^+$ cells (35). We performed tetramer staining on Jurkat-76 cells transduced with the G83.C4 γδ TCR to confirm G83.C4 reactivity to MR1 (35). G83.C4 γδ TCR$^+$ cells displayed strong reactivity to MR1 tetramer in a CD3-dependent fashion (Fig. 2*A* and *SI Appendix*,

Fig. S2), comparable to the MR1-5-OP-RU restricted A-F7 and MR1-autoreactive M33.64 αβ MAIT TCRs (43, 48). The G83.C4 γδ TCR conferred specificity for MR1 presenting 5-OP-RU, with no binding to CD1d presenting α-GalCer (Fig. 2*A*). Next, we assessed the antigen specificity of G83.C4 to MR1 loaded with different metabolite ligands. Interestingly, G83.C4 γδ TCR displayed broad MR1 reactivity, binding to the potent MAIT cell stimulatory ligand 5-OP-RU and the inhibitory ligands Ac-6-FP and 6-FP (Fig. 2*B*) confirming previous observations of MR1 autoreactivity (35). This contrasted with the AF-7 MAIT TCR, which bound exclusively to MR1-5-OP-RU consistent with its antigen-specific reactivity (39). This suggested that the G83.C4 γδ TCR does not recognize MR1 in a ligand-specific manner, consistent with the autoreactive Vδ1/2$^-$ γδ T cells isolated in the blood and duodenum and the autoreactive Vδ1$^+$ T cells previously identified (35).

To gain further insight into the antigen specificity of this Vδ3$^+$ γδ TCR, we purified a soluble form of the G83.C4 TCR and measured the steady-state affinity for MR1 presenting 5-OP-RU, Ac-6-FP, or 6-FP via surface plasmon resonance (SPR). Given the limited expression of the G83.C4 TCR via traditional methods, we generated a δ/α-γ/β chimera wherein the γδ TCR constant domains were replaced with αβ TCR constant domains for bacterial expression (38, 49). The chimeric G83.C4 γδ TCR bound to MR1-5-OP-RU with a high affinity dissociation constant (K_D) of 0.57 ± 0.05 μM, comparable to the A-F7 MAIT TCR 1.75 ± 0.12 μM K_D (Fig. 2*C*). In contrast to the highly specific A-F7 MAIT TCR, which only bound MR1 presenting 5-OP-RU, the G83.C4 TCR exhibited broad MR1 reactivity irrespective of the presented ligand, reminiscent of the previously published Vδ1$^+$ MR1-restricted G7 γδ TCR (35). However, in contrast with the G7 TCR, which bound MR1 with high affinity irrespective of the presented antigen, the G83.C4 γδ TCR showed antigen-dependent affinities to MR1 presenting Ac-6-FP and 6-FP (K_D = 7.83 ± 0.65 and 13.16 ± 1.32 μM, ∼10- and 20-fold changes relative to 5-OP-RU, Fig. 2*C*). These antigen-dependent affinity differences suggested that the G83.C4 γδ TCR may recognize the MR1 antigen-presenting groove instead of the underside as observed for the G7 γδ TCR (35). Thus, the Vδ3$^+$ G83.C4 γδ TCR employs an MR1 recognition mechanism that appears distinct from that of the Vδ1$^+$ G7 γδ TCR and MAIT cell TCRs.

Vδ3Vγ8 TCR-MR1-5-OP-RU Structural Overview. We next determined the structure of the G83.C4 γδ TCR in complex with MR1 presenting 5-OP-RU (Fig. 3*A* and *SI Appendix*, Fig. S3 and Table S2). Here, the G83.C4 γδ TCR bound neither the top nor the underside of the MR1 antigen-binding groove, instead binding on the side of the MR1 α2-helix toward the A′ pocket. G83.C4 γδ TCR employed an orthogonal docking angle (∼90°), whereby the Vδ3 chain sat askew to the MR1 α2-helix and contacted the side of the MR1 antigen-presenting pocket with the Vγ8 chain docked centrally over the α1- and α2-helices (Fig. 3 *D* and *G*). Such a docking mode is unlike that seen for αβ MAIT cell TCR recognition of MR1 that adopted a centralized docking mode atop the antigen-binding groove of MR1 (Fig. 3 *B*, *E*, and *H*) (41, 43, 48, 50). The G83.C4 γδ TCR also stands apart from the G7 Vδ1$^+$ TCR mode of MR1 recognition, sharing no common contacts as it bound underneath the MR1 antigen-binding groove (Fig. 3 *C*, *F*, and *I*) (35). However, the G83.C4 γδ TCR does share contact residues with the αβ MAIT TCR atop the MR1 antigen-presenting pocket (Fig. 3 *G* and *H*), although the Vδ and Vγ chains were shifted ∼30 Å toward the A′ pocket of MR1 relative to the Vα and Vβ respectively.

Although unique, the G83.C4 γδ TCR docking mode did harbor vestiges of the 9C2 γδ TCR mediated recognition of CD1d-α-GalCer (34) (*SI Appendix*, Fig. S4*A*) and the G8 γδ TCR bound to MHC-I–like molecule T22 (51) (*SI Appendix*, Fig. S4*B*). Namely, the 9C2 γδ TCR bound over the A′ pocket of CD1d (34) (*SI Appendix*, Fig. S4*C*) and the T22 autoreactive murine G8 γδ TCR also displayed similar polarization for the MHC-like molecule (*SI Appendix*, Fig. S4*D*). Thus, the Vδ3Vγ8 TCR bound MR1 in a distinct fashion from any other TCR docking modes for MR1.

Molecular Interactions at the G83.C4 γδTCR-MR1-5-OP-RU Interface. The total buried surface area (BSA) of the G83.C4 γδTCR-MR1-5-OP-RU complex was ∼1,970 Å^2, comparable to other γδ TCR complex structures (34, 35, 51) but lower than MAIT TCR-MR1 complexes (41, 45, 48, 50). TCR chain usage was biased toward the Vδ3 chain that contributed 71% of the BSA compared with 29% of the Vγ8 chain. The G83.C4 γδ TCR-MR1-5-OP-RU interface involved contacts from the CDR loops from both the Vδ3-chain (20, 13, and 38% from CDR1δ, CDR2δ, and CDR3δ, respectively) and Vγ8-chain (4, 9, and 16% from CDR1γ, CDR2γ, and CDR3γ, respectively) (Fig. 3 *D* and *G*). Notably, the Vδ-chain dominated the interface, a bias that was also observed in the γδ TCR complexes with CD1d (34), MR1 (35), and T22 (51), which contributed 75, 84, and 89% BSA to the respective interfaces. This theme appears to be a potential emerging paradigm for γδ TCR mediated recognition.

The combination of the Vδ dominated interface and the MR1 side docking means the Vγ of the G83.C4 γδ TCR was distal from the MR1 surface and thus made relatively few contacts to the α1 helix of MR1. Here, the germ-line encoded Y39γ of the CDR1γ made hydrogen bonding contacts with R61 of the α1-helix of MR1 (Fig. 4*A* and *SI Appendix*, Table S3). In addition, Y60γ and N61γ of the CDR2γ contacted the neighboring α1 residues of E60 and D57, respectively (Fig. 4*A*). Although the CDR3γ has been a key mediator of lipid antigen recognition presented in the context of CD1d (34), this was not the case here. Namely, the CDR3γ did not make any direct antigen contacts, instead D106γ, Y107γ, and K108γ contacted N155 and E159 of the α2 helix (Fig. 4*B*).

Many residues contacted by the G83.C4 γδ TCR resided within the α2 helix of MR1 and uniquely, the β4 to 5 loop on the side of MR1 (Fig. 3 *D* and *G*). Such contacts included germ-line encoded CDR1δ and CDR2δ loop contacts with the α2 helix and β4 to 5 loop of MR1, respectively. Key CDR1δ contacts included V29δ, S31δ, and N32δ, which contacted E170, Q177, and K166 of the MR1 α2 helix (Fig. 4*C*). These Vδ3$^+$ specific germ-line contacts are notable as they contrast the comparative residues of Vδ1$^+$ TCR ternary complexes, where W29 and W30 of the CDR1δ played a common and prominent role in ligand recognition (*SI Appendix*, Table S4). Furthermore, another Vδ3 specific germ-line residue, S55δ of the CDR2δ, contacted G104 of the β4 to 5 loop (Fig. 4*C*). This interface was stabilized via dual salt bridge contacts from D34δ and D53δ of the CDR1δ and CDR2δ loops, respectively, that pincered K166 of the α2 helix alongside other contacts (Fig. 4*C*). Thus, many of the germ-line contacts with the α2 helix and β4 to 5 loop of MR1 are potentially unique to Vδ3$^+$ γδ TCRs.

A key mediator of the diverse recognition modes employed by γδ TCRs in recognizing MHC-like molecules has been the CDR3δ loop. This is valid for MR1 recognition by G83.C4 γδ TCR where the CDR3δ loop served as a driver for this unusual docking mode. Here, the CDR3δ made extensive contact with the α2-helix (Fig. 4*D*), mediated via germ-line and non–germ-line encoded residues. Central to this interaction was the encircling of R167 from MR1 by the CDR3δ loop, which was tethered by a salt bridge to D107δ. The encircling of the lynchpin R167 was further stabilized by numerous peripheral contacts mediated by G102δ, P104δ, and H105δ contacting Y171, W164, and E160 of the MR1 α2 helix, respectively.

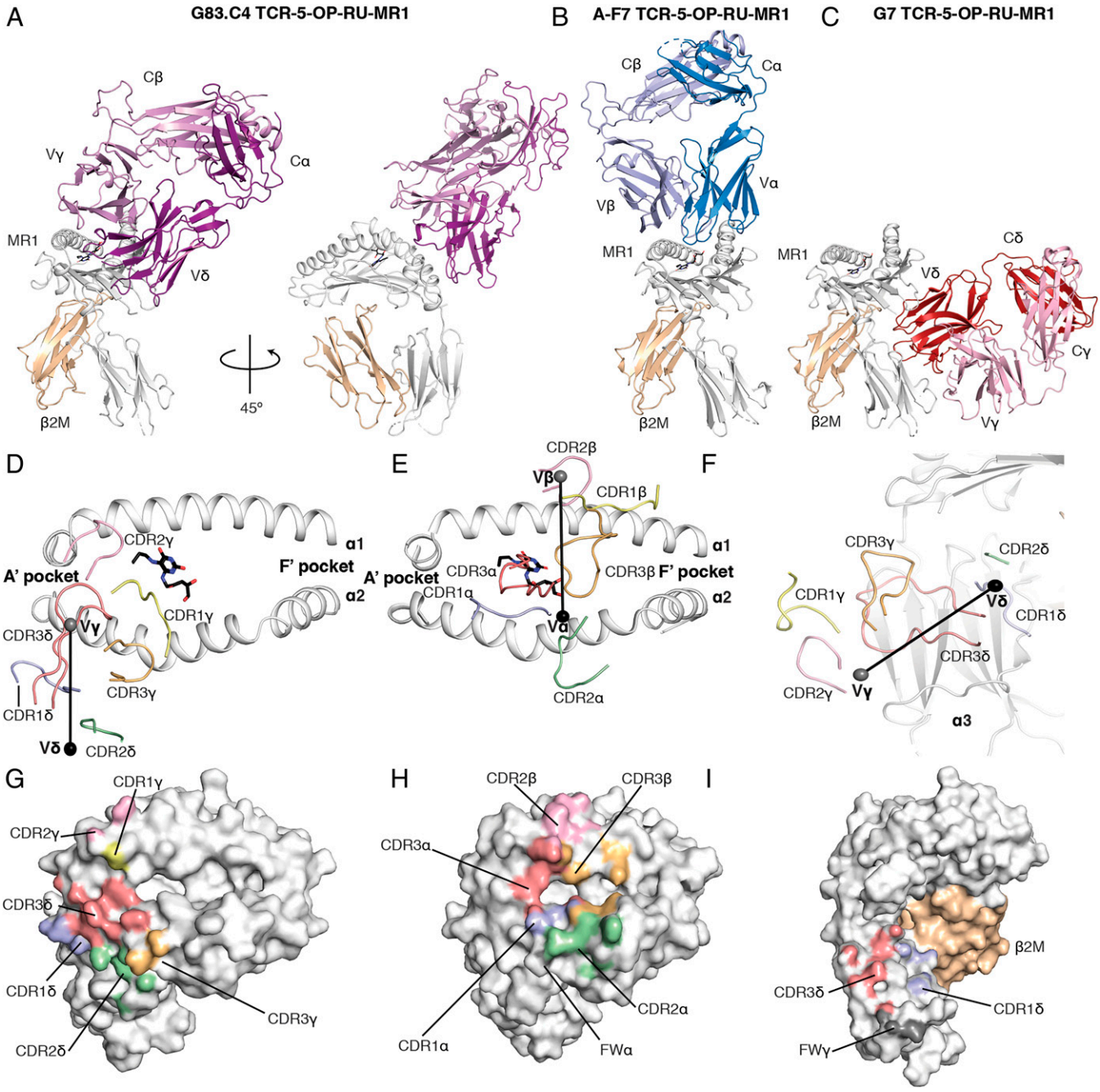

Fig. 3. Overview of the G83.C4 γδ TCR MR1-5-OP-RU complex structure. (*A*) Cartoon representation of the G83.C4 γδ TCR MR1-5-OP-RU, (*B*) A-F7 αβ MAIT TCR MR1-5-OP-RU complex (PDB ID: 4NQC), and (*C*) G7 (Vδ1Vγ9) γδ TCR MR1-5-OP-RU structure (PDB ID: 6MWR) with the TCR δ/α- and γ/β-chains colored dark and light variants of purple, blue, and red, respectively. MR1 and B2M are shown in white and wheat, respectively, with 5-OP-RU is depicted as black sticks. Comparison of the disparate G83.C4 γδ TCR (*D*), A-F7 αβ MAIT TCR (*E*), and G7 γδ TCR (*F*) interfaces and docking modes for MR1-5-OP-RU recognition. The CDR loops are colored as follows: CDR1δ/α light blue, CDR2δ/α green, CDR3δ/α red, CDR1γ/β yellow, CDR2γ/β pink, and CDR3γ/β orange over the MR1 antigen-binding groove. The center of mass of the respective Vδ/α and Vγ/β domains are shown as black and gray spheres, respectively. (*G–I*) The molecular surface of the MR1 molecules is shown with atomic contacts colored according to the respective CDR-loop–mediated interactions.

Despite the extensive TCR-MR1 interface and the moderate sensitivity of G83.C4 γδ TCR to different antigens presented by MR1, there were no direct antigen contacts from the G83.C4 γδ TCR. Given the 30-Å shift of the G83.C4 γδ TCR toward the A′ pocket and the extreme C terminus of the α2-helix, relative to the MAIT TCRs, the result was the occlusion of 5-OP-RU from direct antigen contacts behind an aromatic roof composed of Y62 and W164 (Fig. 4*D*). Indeed, the CDR3δ loop sat directly atop this hydrophobic roof with D103δ and P104δ making extensive electrostatic contacts to Y62 and W164, which is stabilized by the D107δ to R167 salt bridge (Fig. 4*D*). Thus, the Vδ3 of the G83.C4 γδ TCR confers much of the reactivity to MR1 via the CDR3δ loop most notably with R167 and the aromatic roof of the MR1 antigen-binding groove. Accordingly, the Vδ3$^+$ G83.C4 γδ TCR employed an MR1 binding mode that was distinct from that of the Vδ1$^+$ G7 γδ TCR and MAIT TCRs described to date.

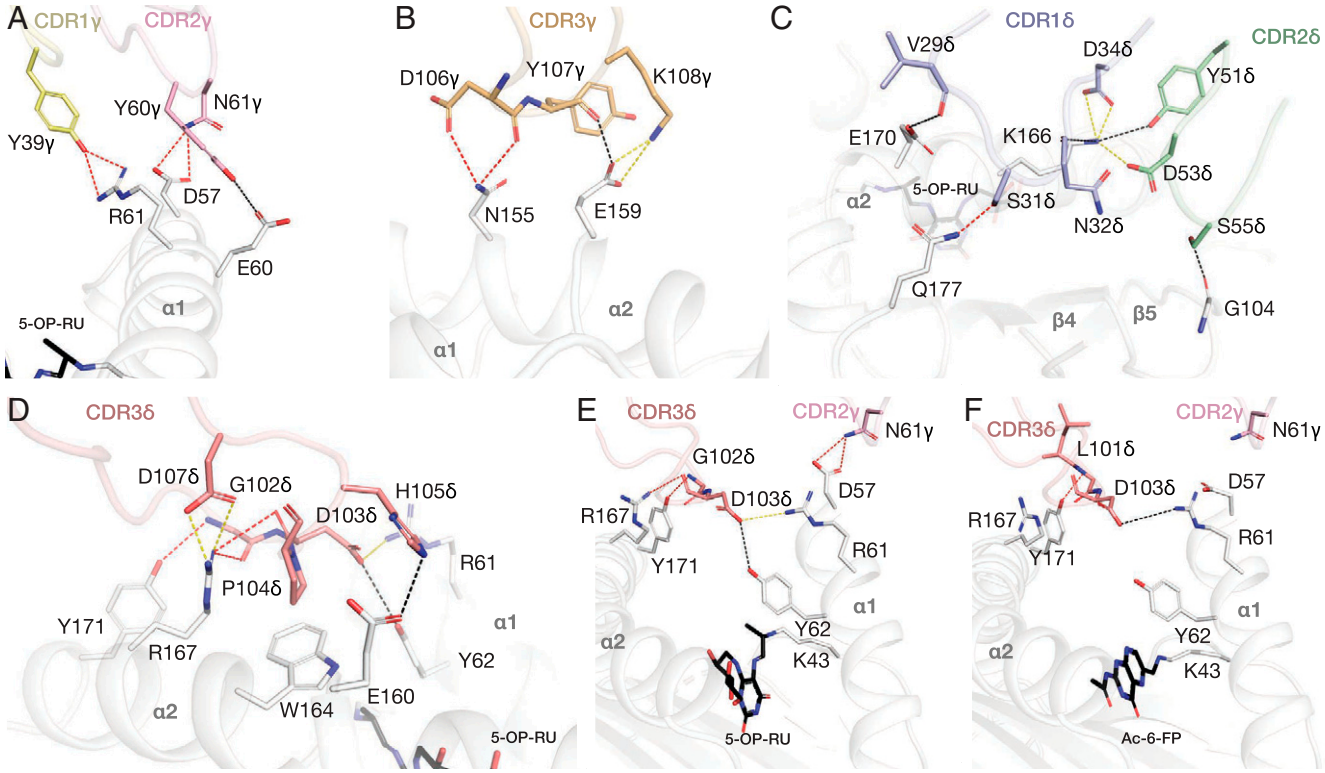

Fig. 4. Molecular interactions at the G83.C4 TCR MR1-5-OP-RU interface. (*A*) Molecular interactions of the CDR1γ, CDR2γ, and CDR3γ (*B*) loops and MR1. (*C*) Molecular interactions of the G83.C4 δ-chain to the side of MR1 antigen-presenting pocket via CDR1δ, CDR2δ, and CDR3δ (*D*) mediated contacts. MR1 is colored white, and 5-OP-RU shown as black sticks in all panels. (*E*) Comparison of the antigen-specific changes within the G83.C4 TCR bound to MR1 bound to 5-OP-RU and MR1 bound Ac-6-FP (*F*). The CDR loops are colored according to Fig. 3. Hydrogen, salt bridge, and van der Waals contacts are shown by red, yellow, and black dashed lines, respectively.

Antigen-Dependent Impact on the G83.C4 γδ TCR-MR1 Interaction. Although the G83.C4 γδ TCR bound MR1 without direct ligand contact, our initial biochemical analysis suggested some antigen-dependent effect upon TCR recognition (Fig. 2*C*). To elucidate the molecular basis for this altered affinity, we determined the structure of the G83.C4 γδ TCR in complex with the lower affinity ligand Ac-6-FP presented by MR1 (*SI Appendix*, Figs. S5 and S6 and Table S2). Despite an ∼10-fold lower affinity for MR1-Ac-6-FP, the G83.C4 γδ TCR adopted the same overall docking mode with many of the molecular contacts from the 5-OP-RU structure being retained (*SI Appendix*, Fig. S5).

Indeed, only modest rearrangements occurred at the molecular interface and were distal from the antigen. Here, the altered contacts were primarily associated with the CDR2γ and CDR3δ loops (Fig. 4 *E* and *F*) with a loss of backbone contacts from the CDR1γ to the α1 of MR1 and a similar loss of contacts to the α1 and α2 helices of MR1 by CDR3δ (Fig. 4*F* and *SI Appendix*, Table S5). D57, which sat over the α2 helices of MR1 when presenting 5-OP-RU, rotated centrally when presenting Ac-6-FP, leading to disruption of contacts with N61γ. Similarly, R61 and Y62 rotate away from the A′ pocket of MR1, when presenting Ac-6-FP, resulting in a breakdown of contacts with D103δ and disrupting CDR3δ H-bonding. These subtle CDR2γ and CDR3δ changes are unlikely to solely account for the reduced affinity, instead they may be symptomatic rather than deterministic and we hypothesize a combination of MR1 plasticity (*SI Appendix*, Fig. S6 *A* and *B*) and stability (*SI Appendix*, Fig. S6 *C–E*), when presenting different ligands may drive the affinity differences (39, 41). Alignment of unliganded MR1-6-FP (44) to MR1-5-OP-RU and Ac-6-FP complexed to G83.C4 suggest that the α2 helices and β4 to 5 loop are dynamic (*SI Appendix*, Fig. S6 *A* and *B*) and shift upon G83.C4 γδ TCR ligation, a feature conserved with MAIT TCRs (41). Thus, in the absence of direct antigen contacts, presentation of different metabolite antigens by MR1 may change the flexibility of the α2 helix (*SI Appendix*, Fig. S6 *F* and *G*), impacting the ability of G83.C4 to bind MR1.

A Reliance of Vδ3 CDR3δ Loop for MR1 Recognition. To date, no other Vδ3$^+$ γδ TCR complex structures have been determined. We undertook mutagenesis experiments to identify the key determinants of Vδ3$^+$ G83.C4 γδ TCR recognition of MR1 in both cellular and biochemical context. We conducted structure-guided mutation of 10 residues within the MR1 epitope recognized by the G83.C4 γδ TCR (D57A, E60A, R61E, G104A, N155A, E159A, E160A, W164A, R167A, and Y171A) alongside a control mutant proximal to the interface (T106A) and mutations within the α3 (Mut5X) known to ablate underside docking.

Initially, we performed tetramer staining of TCR-transduced Jurkat-76 cells, expressing the G83.C4 γδ TCR or the control αβ MAIT TCRs M33.64 and A-F7 (Fig. 5*A*). Mutations of MR1 α1 helix corresponding to γ-chain mediated contacts (D57A and E60A) generally had little impact. Notwithstanding R61E, which corresponded to a 10-fold decrease in tetramer binding (Fig. 5 *A* and *B*). Given that R61 was involved in contacts with both the CDR1γ via a hydrogen bond contact with Y39γ, and a salt bridge contact with D103δ of CDR3δ, of the G83.C4 γδ TCR, it is not surprising that this charge reversal mutant disrupted TCR binding.

Conversely, mutation of α2 helix residues corresponding to δ-chain contacts had differing impacts on TCR binding.

Mutation of residues peripheral to the interface had little impact on G83.C4 binding (N155A, E159A, and E160A), whereas mutation of G104A, a key residue within the β4 to 5 loop on the side of the MR1 antigen-presenting groove, moderately impacted G83.C4 binding. Disruption of W164A and R167A, which formed stacking interaction with P104δ and salt bridge with D103δ, respectively, MR1 residues of central importance to CDR3δ contacts completely ablated G83.C4 γδ TCR binding. Furthermore, disruption of the residue neighboring R167, namely a Y171A mutation, had a moderate impact on the G83.C4 binding despite mainly serving to stabilize R167 at the interface. Notably, mutation of key residues (R61E and W164A) that overlap with the 'top docking MR1 footprint also impacted the control TCRs. In addition, the T106A and Mut5X, which included five mutations within the MR1 α3 domain that ablates underside recognition, had no impact on the G83.C4 γδ TCR binding (35). Furthermore, when looking at normalized tetramer staining intensity the R61E, W164A, and R167A mutations completely disrupted binding to the G83.C4 γδ TCR (Fig. 5*B*).

We validated our cellular findings via SPR experiments (Fig. 5 *C–F* and *SI Appendix*, Figs. S7 and S8) (52). We confirmed that the R61E mutation ablated TCR binding, as it caused a >10-fold decrease in both G83.C4 and A-F7 MAIT TCR affinity (Fig. 5 *C* and *D*). We also found that the D57 mutation reduced the affinity of the G83.C4 γδ TCR threefold, $K_D = 2.62 \pm 0.96$ μM, which we had not observed by tetramer staining (Fig. 5*C*). We also confirmed the increased sensitivity of the G83.C4 γδ TCR to Vδ contact residue mutagenesis. Here, the G104A mutation moderately impacted G83.C4 γδ TCR affinity ($K_D = 6.91 \pm 0.97$ μM) (Fig. 5*C*). More strikingly, both W164A and R167A severely impacted G83.C4 γδ TCR affinity for MR1 with 50- to 100-fold decreases in affinity, further validating our tetramer staining results (Fig. 5*C*). Additionally, mutagenesis of Y171 results in a sevenfold reduction in affinity ($K_D = 6.37 \pm 1.42$ μM).

Collectively, these results highlight that MR1 recognition by this Vδ3$^+$ γδ TCR hinged on a defined subset of MR1 residues contacted most notably by the CDR3δ loop, which contributed 40% of the interface BSA. Notable germ-line residues unique to the Vδ3 gene played a role in this unique interface including CDR1δ and CDR2δ residues, which converged on K166 of the MR1 α2 helix. Furthermore, the Vδ3-specific CDR2δ residues S55 and R56 mediated key contacts to G104 of the β4 to 5 loop. Ostensibly, the CDR3δ was shown to be the key mediator of the unique docking topology of G83.C4 with numerous residues converging on R167 of the MR1 α2 helix.

Spectratyping and CDR3 analysis of the blood ($n = 2$) and duodenal ($n = 2$) Vδ2-γδ T cell repertoires showed no focusing within the duodenum for the non–germ-line CDR3δ residues that are central to this docking mode. To probe the generality of the G83.C4 (Vδ3/Vγ8) TCR, we next analyzed the CDR3 length of the total TCR repertoire and the CDR3 identity to G83.C4 within similar length Vδ3 and Vγ8 TCRs (*SI Appendix*, Fig. S9). These data highlighted a diverse CDR3 length and low sequence identity to the G83.C4 γδ TCR. Thus, although germ-line Vδ3$^+$-specific contacts were evident, the hypervariable CDR3δ loop endowed the G83.C4 clone with the ability to bind MR1 in such a unique manner. The lack of CDR3δ loop focusing could suggest that the wider Vδ3$^+$ γδ T cell subset likely recognizes antigens via distinct mechanisms beyond those described here.

Discussion

The relative lack of bona fide γδ T cell antigens has hindered the understanding of their role in human immunity. To date, γδ T cells have been shown to interact with the CD1 family, EPCR, MHC, and MR1 (32–35, 37). However, structural and phenotypical analysis has primarily focused on the Vδ1$^+$ and Vδ2$^+$ γδ T cell subsets, despite Vδ3$^+$ γδ T cells being a major constituent of IELs within the gut mucosa (24). The identification of Vδ3$^+$ MR1-reactive γδ T cell clones (35) expanded our knowledge of Vδ3$^+$ γδ T cell ligands beyond CD1d and annexin A2 reactivity (26, 53). We identified MR1-tetramer$^+$ Vδ3$^+$ γδ T cells both within the blood and gut epithelial tissue of children and young adults. The gut γδ T cell population expressed a more diverse TCR repertoire than the circulating Vδ3$^+$ MR1-tetramer$^+$ γδ T cells. With MR1-reactive T cells implicated in viral (54) and bacterial (55) clearance, as well as TCR mediated antitumor responses (56), it remains unknown whether Vδ3$^+$ γδ T cells display a similar breadth of immunological and effector function.

Here, we identified a clonally unfocused Vδ2$^-$ T cell population across healthy and patient-derived samples. In the blood, we found an enrichment of Vδ1$^+$ TCR sequences and rarefied Vδ3$^+$ γδ TCR sequences. Conversely in the duodenum, Vδ1 and Vδ3 sequences were more equal in frequency. Notably these observations persisted across healthy and patient-derived samples. We identified blood and tissue Vδ1/2$^-$ γδ T cells that stained with both 5-OP-RU and 6-FP–loaded MR1 tetramers. Previous analysis of the MR1-reactive Vδ3$^+$ γδ T cell repertoire revealed a clone (G83.C4) that was autoreactive toward MR1 (35). Biophysical analysis of this clone highlighted some element of antigen-specific recognition, whereby the G83.C4 clone preferentially bound the stimulatory MR1-5-OP-RU over the MAIT cell antagonists Ac-6-FP and 6-FP. Furthermore, we determined the structure of a Vδ3$^+$ γδ TCR bound to MR1 that showed the γδ TCR diverged from the classical 'top docking MR1 recognition displayed by the MAIT αβ TCR. Here, the Vδ3 chain directed MR1 contacts over the A′ pocket, adopting a highly unusual docking mode contacting the side of MR1. This docking mode was distinct from conventional and atypical MAIT TCRs as well as Vδ1$^+$ G7 γδ TCR recognition of MR1 (35, 48, 57).

As with the Vδ1$^+$ G7 γδ TCR, the G83.C4 γδ TCR bound distal to the presented antigen and made no direct contact with the ligands. Thus, the antigen recognition pathway of γδ T cells seems to stand apart from that of conventional αβ T cells and may suggest an autoreactivity role that recognizes protein surface expression as seen for unconventional αβ T cell lipid-mediated reactivities although the ligand dependencies seem distinct (58, 59). Indeed, MR1 surface expression is a tightly regulated process (60, 61) with cell-surface expression linked to MR1-ligand availability (39, 46, 55).

Intriguingly, although the G83.C4 γδ TCR bound away from the presented antigen, a modest decrease of the steady-state affinity was observed for MR1-Ac-6-FP relative to 5-OP-RU as observed for MR1-reactive Vδ1$^+$ γδ TCRs (35). We speculate that this subtle antigen-dependent effect upon affinity results from differing structural resonances and plasticity of the MR1 antigen-binding groove when bound to different ligands. Structural analyses have highlighted modest changes within the MR1 antigen-binding groove when presenting different ligands, including Q153 as identified here, but further non-TCR bound MR1 structures will be key to validating this hypothesis (39).

Another interesting observation of the G83.C4 γδ TCR–MR1 structure was the δ-chain dominance in γδ T cell mediated antigen recognition. This striking δ-chain dominance is observed in all γδ TCR ligand structures solved to date and well conserved across different MHC-like molecules at ∼75 to 90% of the total interface area (34, 35, 51, 62). This theme remained consistent for the Vδ3-mediated recognition of MR1 where the main drivers of the interface were non–germ-line encoded CDR3δ residues, which contributed ∼40% of the BSA. Given the CDR3 loops within the Vδ2$^-$ population bore incredible diversity, and that these regions play a central role in this unique docking

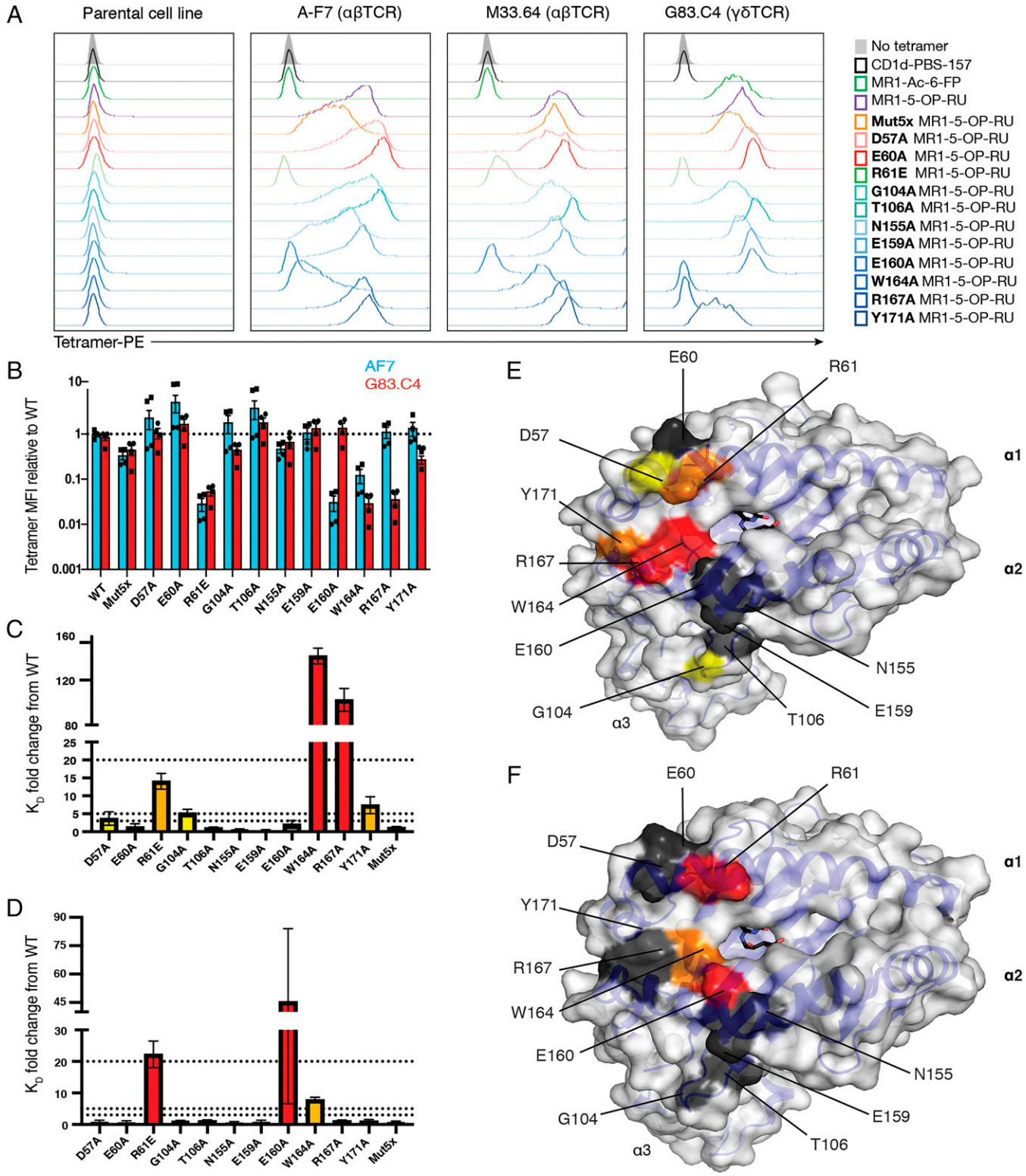

Fig. 5. Key molecular determinants of Vδ3Vγ8 TCR MR1 recognition. (*A*) Flow cytometry histograms showing tetramer staining with MR1-5-OP-RU mutants on Jurkat-76 parental or transduced with A-F7 and M33.64 αβ MAIT or G83.C4 γδ TCRs. (*B*) Mean fluorescence intensity (MFI) of tetramer staining with MR1-5-OP-RU mutants, relative to wild-type (WT) MR1-5-OP-RU staining of transduced Jurkat cells with G83.C4 and A-F7. Bar is at the mean and error bars represent SD between technical duplicates. Results are representative of at least two independent experiments. (*C*) Fold difference of G83.C4 and A-F7 (*D*) binding affinity determined via SPR of MR1-5-OP-RU mutants. Bar is at the equilibrium dissociation constant (K_D) fold difference relative to WT MR1-5-OP-RU. Error bars denote SD from two independent experiments, performed in duplicate. Yellow bar denotes >threefold change. Orange bar depicts >fivefold change. Red bar denotes >20-fold change. (*E* and *F*) Impact of MR1 mutagenesis on TCR binding mapped onto the surface of MR1. MR1 surface, white; MR1 cartoon representation, blue; residue color based on affinity impact in *C* and *D*. Gray denotes a <threefold impact on TCR affinity.

mode, the implication is that Vδ3$^+$ γδ TCRs may recognize MR1 and other antigens by diverse mechanisms beyond that of the G83.C4 γδ TCR.

Here, we show that a diverse subset of Vδ1/2$^-$ T cells broadly bound MR1-tetramers and defined how one Vδ3$^+$ γδ TCR mediated antigen-independent recognition of MR1. The structures solved here further strengthen the hypothesis of how γδ TCRs utilize atypical recognition modes for antigen recognition. The structures also solidify the paradigm of antibody-like recognition of MR1 by γδ T cells and underscores the suggestion that antigen recognition modes may in fact be clonally unique among γδ T cells. Indeed, together these data reinforce the idea that γδ TCRs may not converge upon specific interfaces with broad consensus mechanisms like αβ T cell restrictions. Instead, γδ diversity may enable antigen recognition by molecular interactions that may be potentially unique and private to a γδ TCR-antigen pairing. This was postulated for the Vδ1$^+$ lineage and will only become clearer as we identify and characterize the eclectic reactivity of γδ T cells more broadly. Given the limited knowledge regarding the abundance and diversity of Vδ3$^+$ γδ T cells in key immunological sites, the identification of other Vδ3$^+$ γδ T cell ligands may further clarify the importance of these cells in humans.

Materials and Methods

Study Population. Matched blood and duodenum biopsies were taken from consenting patients undergoing routine endoscopy procedures at Monash Children's Hospital, Melbourne (*SI Appendix*, Table S1). Celiac disease or IBD was diagnosed by clinical and laboratory evaluation, including serological and histologic assessment. This study was approved by Monash Health research ethics committee (HREC/16/MonH/253).

Peripheral Blood Mononuclear Cell Isolation. Venous blood was diluted 1:1 in phosphate buffered saline (PBS) and was layered over lymphoprep (Stemcell Technologies) and gradient centrifuged for 20 mins at 600 × *g* at room temperature (RT) without brake. The resulting peripheral blood mononuclear cells (PBMCs) layer was washed twice in Rosswell Memorial Park Institute (RPMI)-1640 medium for 10 min at 400 × *g* at RT with brake 6.

Duodenal Biopsy Culture. Duodenal biopsies were rinsed in RPMI-1640 medium supplemented with 10% fetal calf serum, 1:100 penicillin, streptomycin, and amphotericin B, 1% nonessential amino acids, and 0.6% gentamycin (complete medium). Whole biopsies were cultured for 10 d in complete medium in the presence of 100 u/mL IL-2 and 10 ng/mL IL-15 (Miltenyi Biotec). Emigrating lymphocytes were then subject to flow cytometry analysis, TCR repertoire sequencing, and MR1-tetramer staining.

Flow Cytometry of Human Samples. Uncultured human PBMCs and 10-d cultured duodenal cells were stained with 1:500 diluted Zombie Aqua fixable viability dye (Biolegend). Next, cells were stained with anti-human CD3-BUV395 (UCHT1, BD), γδTCR-APC-Vio770 (REA594), Vδ1-FITC (REA173), and Vδ2-APC (123R3), all from Miltenyi Biotec; and CD69-BV650 (FN50) and CD103-PerCP/Cy5.5 (Ber-ACT8), all from Biolegend. Cells from the peripheral blood or duodenal biopsies of five donors were also stained with MR1-5-OP-RU or 6-FP tetramers conjugated to APC or BV421 (1:100) for 15 min at RT before staining with other surface markers. Flow cytometry data were collected on a BD LSRFortessa X20 (BD). Data were analyzed using FlowJo cell analysis software (FlowJo, LLC).

Bulk Vγ9/Vδ2$^-$ T Cell Sorting and TCR Sequencing. Uncultured human PBMCs and 10-d cultured duodenal cells were stained with Zombie Aqua fixable viability dye as described in Fig. 1 and *SI Appendix*, Fig. S1. Cells were then stained with anti-human CD3-BUV395, γδTCR-APC-Vio770, αβTCR-Vioblue (REA652, Miltenyi Biotec), Vδ1-FITC, Vγ9-PC5 (IMMU360, Beckman Coulter), and Vδ2-APC for 20 mins on ice in magnetic cell separation buffer (PBS supplemented with 2% fetal calf serum and EDTA). Vγ9/Vδ2$^-$ T cells were bulk sorted using a BD FACSAria Fusion cell sorter (BD Biosciences) into RNA*later* (Sigma-Aldrich). RNA was purified using an RNeasy plus micro kit (Qiagen) following the manufacturer's instructions. The human TCR δ and γ iRprofile kits (iRepertoire Inc) were used to prepare CDR3δ and CDR3γ libraries for sequencing, following instructions from the manufacturer. TCR libraries were pooled and sequenced using an Illumina MiSeq (Micromon Genomics or Monash Health Translation Precinct genomics facility, Monash University, Melbourne, Australia). CDR3 sequences and variable (V), diversity (D), and junction (J) gene usage were identified, and tree maps were generated using iRweb tools (iRepertoire Inc.). Within tree maps, each unique CDR3 region is assigned to a colored segment, with the size of the rectangle corresponding to the abundance of each CDR3 within the total TCR repertoire. Sequence logos were generated on the WebLogo 3 (63) platform and give a visual representation of amino acids enriched at different positions in the observed CDR3 sequences. The different amino acids are colored according to physicochemical properties with polar (G, S, T, Y, C), neutral (Q, N), basic (RKH), acidic (D, E), and hydrophobic (A, V, L, I, P, W, F, M) residues colored green, purple, blue, red, and black, respectively.

MR1 and CD1d Tetramer Generation. Biotinylation and tetramer generation of human MR1 and CD1d tetramers were generated as previously described (42, 43, 64).

Tetramer Staining Jurkat Cell Lines. Cells were first stained with viability dye LIVE/DEAD Fixable Aqua Dead Cell Stain Kit (Life Technologies) for 10 min at RT. Cells were then incubated with MR1 PE tetramers diluted 1:100 in PBS with 10% fetal bovine serum (FBS) (Sigma) for 15 min at RT. Cells were then stained with PE/Cy7 anti-human CD3 (UCHT-1, Biolegend) diluted in PBS/10% FBS for 20 min on ice. Flow cytometry data were collected on a BD LSRFortessa X20. Data were analyzed using FlowJo cell analysis software (FlowJo, LLC).

Generation of Soluble TCRs and MR1. G83.C4 δ/α, γ/β were cloned into pET-30b with the resultant inclusion bodies produced as described previously (38, 49). G83.C4 was refolded via the addition of 100 mg δ/α and γ/β to a 1-L refolding solution containing 100 mM Tris pH 8.5, 1 mM oxidized glutathione 2 mM EDTA, 0.2 mM PMSF, 5 M Urea, 0.4 mM L-arginine, and 5 mM reduced glutathione for 48 h at 4 °C. The resultant refold solution was then dialyzed against 10 mM Tris · HCl pH 8.5 and purified via Macro-Prep DEAE (Sigma-Aldrich) and eluted in 10 mM Tris · HCl pH 8.5 and 400 mM NaCl, which was then concentrated and purified via anion exchange chromatography over a Hi-TrapQ HP (GE Healthcare). A final hydrophobic interactivity column was performed with a 1 mL HiTrap-Phenyl HP (GE Healthcare). Sodium dodecyl sulfate–polyacrylamide gel electrophoresis was used to assess protein purity at each stage, and the final protein concentration was determined with a Nanodrop 1000 spectrophotometer (Thermo Scientific), measured at 280 nm. A-F7 TCR was expressed and purified as previously described (45). Soluble MR1 and β_2M were expressed and refolded with either 5-OP-RU or Ac-6-FP via previously established methods (39, 43). The 5-OP-RU ligand was generated in situ from the addition of 5-A-RU and methylglyoxal as previously described (43).

Crystallization, Structural Determination, and Refinement. G83.C4 and MR1-5-OP-RU or MR1-Ac-6-FP were incubated overnight at 4 °C at 100:100 μM. Size-exclusion chromatography was performed via SE 200 10/30 (GE Healthcare) to remove monomer species. Fractions corresponding to cocomplexed protein were pooled and concentrated to 5 mg/mL for crystallization trials. Both G83.C4-MR1-5-OP-RU and G83.C4-MR1-Ac-6-FP ternary complexes crystallized in 30 to 40% PEG 400, 0.1/0.2 M Hepes pH 7.5, and 0.2 M $MgCl_2$. Crystals were flash frozen and imaged at the Australian Synchrotron MX2 beamline (65). Image files were processed using XDS and the CCP suite of programs (66). Molecular replacement using MR1 and β2M structure (Protein Data Bank [PDB] accession code: 4GUP), the αβ constant region from 4NQC (48) and the Vδ3 chain from 1TVD (68), the Vγ9 from 6MWR (35) with the CDR loops removed as four separate searches were conducted in Phenix (67). An initial round of refinement was performed followed by manual rebuilding of the CDR loops via COOT (69). Two complexes were present within the asymmetric unit, with clear ligand density for both 5-OP-RU and Ac-6-FP present for the respective structures. Following iterative model building using Phenix 1.17.1, the G83.C4-MR1-5-OP-RU was refined to an R_{work}/R_{free} of (%) 24.00/26.10 while G83.C4-MR1-Ac-6-FP was refined to 24.34/27.68. All structural graphics were prepared using PyMOL (70).

SPR. SPR experiments were performed using a BIACore T3000 at 25 °C in Hepes buffer saline buffer (20 mM Hepes-HCl pH 7.4, 150 mM NaCl). Biotinylated MR1 was coupled to a streptavidin chip (GE Healthcare) to ∼2,000 response units with δ/α-γ/β TCR G83.C4 and αβ MAIT A-F7 TCR used as the analyte at concentrations ranging from 200 to 0 μM. Biotinylated MR1 mutants were refolded with 5-OP-RU. GraphPad Prism 8 was used to generate graphical representations of sensorgrams and affinity curves.

Statistical Analysis. Tabulated data were analyzed in GraphPad Prism 9 (GraphPad Software, Inc.). Each dataset was first assessed for normality using

Shapiro–Wilk normality test and then a paired *t* test was performed to analyze differences between blood and duodenum.

Data Availability. The atomic coordinates and structure factors have been deposited in the PDB (PDB ID codes: 7LLI and 7LLJ). The raw sequencing data for the γδTCR repertoires are available in Open Science Framework at https://osf.io/7ptve/. All other study data are included in the article and/or *SI Appendix*.

ACKNOWLEDGMENTS. We thank the staff of the Monash Molecular Crystallisation Facility for their assistance. This research was supported by the National Health and Medical Research Council (NHMRC; Australia), the Australian Research Council (ARC; Grant DP200103462 to B.S.G.), and the National Institute of Allergy and Infectious Diseases of the NIH (Grant R01AI148407 to J.R.). J.R. is supported by an ARC Australian Laureate Fellowship. D.I.G. is supported by an NHMRC Senior Principal Research Fellowship. M.S.D. is supported by an ARC Discovery Early Career Researcher Award. The human patient analysis was funded by Rebecca L. Cooper Medical Research Foundation Project Grant PG2020668 and by the ARC Discovery Project (Grant DP210103327 to J.L.N. and M.S.D.). This research was undertaken in part using the MX2 beamline at the Australian Synchrotron, part of the Australian Nuclear Science and Technology Organisation, and made use of the Australian Cancer Research Foundation detector. We thank staff of the FlowCore and Micromon platforms for their assistance.

1. J. Zheng, Y. Liu, Y.-L. Lau, W. Tu, γδ-T cells: An unpolished sword in human anti-infection immunity. *Cell. Mol. Immunol.* **10**, 50–57 (2013).
2. B. Silva-Santos, K. Serre, H. Norell, γδ T cells in cancer. *Nat. Rev. Immunol.* **15**, 683–691 (2015).
3. P. Vantourout, A. Hayday, Six-of-the-best: Unique contributions of γδ T cells to immunology. *Nat. Rev. Immunol.* **13**, 88–100 (2013).
4. G. De Libero *et al.*, Selection by two powerful antigens may account for the presence of the major population of human peripheral gamma/delta T cells. *J. Exp. Med.* **173**, 1311–1322 (1991).
5. T. Dimova *et al.*, Effector Vγ9Vδ2 T cells dominate the human fetal γδ T-cell repertoire. *Proc. Natl. Acad. Sci. U.S.A.* **112**, E556–E565 (2015).
6. F. Davodeau *et al.*, Peripheral selection of antigen receptor junctional features in a major human γδ subset. *Eur. J. Immunol.* **23**, 804–808 (1993).
7. C. M. Parker *et al.*, Evidence for extrathymic changes in the T cell receptor gamma/delta repertoire. *J. Exp. Med.* **171**, 1597–1612 (1990).
8. C. T. Morita, C. Jin, G. Sarikonda, H. Wang, Nonpeptide antigens, presentation mechanisms, and immunological memory of human Vγ2Vδ2 T cells: Discriminating friend from foe through the recognition of prenyl pyrophosphate antigens. *Immunol. Rev.* **215**, 59–76 (2007).
9. G. Costa *et al.*, Control of *Plasmodium falciparum* erythrocytic cycle: γδ T cells target the red blood cell-invasive merozoites. *Blood* **118**, 6952–6962 (2011).
10. A. Sandstrom *et al.*, The intracellular B30.2 domain of butyrophilin 3A1 binds phosphoantigens to mediate activation of human Vγ9Vδ2 T cells. *Immunity* **40**, 490–500 (2014).
11. C. Harly *et al.*, Key implication of CD277/butyrophilin-3 (BTN3A) in cellular stress sensing by a major human γδ T-cell subset. *Blood* **120**, 2269–2279 (2012).
12. D. A. Rhodes *et al.*, Activation of human γδ T cells by cytosolic interactions of BTN3A1 with soluble phosphoantigens and the cytoskeletal adaptor periplakin. *J. Immunol.* **194**, 2390–2398 (2015).
13. M. Rigau *et al.*, Butyrophilin 2A1 is essential for phosphoantigen reactivity by γδ T cells. *Science* **367**, eaay5516 (2020).
14. M. S. Davey *et al.*, The human $V\delta2^+$ T-cell compartment comprises distinct innate-like $V\gamma9^+$ and adaptive $V\gamma9^-$ subsets. *Nat. Commun.* **9**, 1760 (2018).
15. C. T. Morita, C. M. Parker, M. B. Brenner, H. Band, TCR usage and functional capabilities of human gamma delta T cells at birth. *J. Immunol.* **153**, 3979–3988 (1994).
16. K. Deusch *et al.*, A major fraction of human intraepithelial lymphocytes simultaneously expresses the γ/δ T cell receptor, the CD8 accessory molecule and preferentially uses the V δ 1 gene segment. *Eur. J. Immunol.* **21**, 1053–1059 (1991).
17. P. Brandtzaeg *et al.*, T lymphocytes in human gut epithelium preferentially express the α/β antigen receptor and are often CD45/UCHL1-positive. *Scand. J. Immunol.* **30**, 123–128 (1989).
18. J. D. Bos *et al.*, T-cell receptor gamma delta bearing cells in normal human skin. *J. Invest. Dermatol.* **94**, 37–42 (1990).
19. V. Groh, A. Steinle, S. Bauer, T. Spies, Recognition of stress-induced MHC molecules by intestinal epithelial γδ T cells. *Science* **279**, 1737–1740 (1998).
20. D. V. Correia *et al.*, Differentiation of human peripheral blood Vδ1+ T cells expressing the natural cytotoxicity receptor NKp30 for recognition of lymphoid leukemia cells. *Blood* **118**, 992–1001 (2011).
21. K. Hudspeth *et al.*, Engagement of NKp30 on Vδ1 T cells induces the production of CCL3, CCL4, and CCL5 and suppresses HIV-1 replication. *Blood* **119**, 4013–4016 (2012).
22. M. S. Davey *et al.*, Clonal selection in the human Vδ1 T cell repertoire indicates γδ TCR-dependent adaptive immune surveillance. *Nat. Commun.* **8**, 14760 (2017).
23. M. S. Davey, C. R. Willcox, A. T. Baker, S. Hunter, B. E. Willcox, Recasting human Vδ1 lymphocytes in an adaptive role. *Trends Immunol.* **39**, 446–459 (2018).
24. M. C. Falk *et al.*, Predominance of T cell receptor Vδ3 in small bowel biopsies from coeliac disease patients. *Clin. Exp. Immunol.* **98**, 78–82 (1994).
25. M. R. Dunne *et al.*, Persistent changes in circulating and intestinal γδ T cell subsets, invariant natural killer T cells and mucosal-associated invariant T cells in children and adults with coeliac disease. *PLoS One* **8**, e76008 (2013).
26. B. A. Mangan *et al.*, Cutting edge: CD1d restriction and Th1/Th2/Th17 cytokine secretion by human Vδ3 T cells. *J. Immunol.* **191**, 30–34 (2013).
27. E. Robak *et al.*, Lymphocyctes Tgammadelta in clinically normal skin and peripheral blood of patients with systemic lupus erythematosus and their correlation with disease activity. *Mediators Inflamm.* **10**, 179–189 (2001).
28. E. Robak *et al.*, Circulating TCR γδ cells in the patients with systemic lupus erythematosus. *Mediators Inflamm.* **8**, 305–312 (1999).
29. J. Déchanet *et al.*, Implication of γδ T cells in the human immune response to cytomegalovirus. *J. Clin. Invest.* **103**, 1437–1449 (1999).
30. J. L. Taupin *et al.*, An enlarged subpopulation of T lymphocytes bearing two distinct γδ TCR in an HIV-positive patient. *Int. Immunol.* **11**, 545–552 (1999).
31. P. M. Benveniste *et al.*, Generation and molecular recognition of melanoma-associated antigen-specific human γδ T cells. *Sci. Immunol.* **3**, eaav4036 (2018).
32. J. F. Reijneveld *et al.*, Human γδ T cells recognize CD1b by two distinct mechanisms. *Proc. Natl. Acad. Sci. U.S.A.* **117**, 22944–22952 (2020).
33. S. Roy *et al.*, Molecular analysis of lipid-reactive Vδ1 γδ T cells identified by CD1c tetramers. *J. Immunol.* **196**, 1933–1942 (2016).
34. A. P. Uldrich *et al.*, CD1d-lipid antigen recognition by the γδ TCR. *Nat. Immunol.* **14**, 1137–1145 (2013).
35. J. Le Nours *et al.*, A class of γδ T cell receptors recognize the underside of the antigen-presenting molecule MR1. *Science* **366**, 1522–1527 (2019).
36. X. Zeng *et al.*, γδ T cells recognize a microbial encoded B cell antigen to initiate a rapid antigen-specific interleukin-17 response. *Immunity* **37**, 524–534 (2012).
37. C. R. Willcox *et al.*, Cytomegalovirus and tumor stress surveillance by binding of a human γδ T cell antigen receptor to endothelial protein C receptor. *Nat. Immunol.* **13**, 872–879 (2012).
38. A. M. Luoma *et al.*, Crystal structure of Vδ1 T cell receptor in complex with CD1d-sulfatide shows MHC-like recognition of a self-lipid by human γδ T cells. *Immunity* **39**, 1032–1042 (2013).
39. S. B. G. Eckle *et al.*, A molecular basis underpinning the T cell receptor heterogeneity of mucosal-associated invariant T cells. *J. Exp. Med.* **211**, 1585–1600 (2014).
40. M. Lepore *et al.*, Parallel T-cell cloning and deep sequencing of human MAIT cells reveal stable oligoclonal TCRβ repertoire. *Nat. Commun.* **5**, 3866 (2014).
41. O. Patel *et al.*, Recognition of vitamin B metabolites by mucosal-associated invariant T cells. *Nat. Commun.* 4, 2142 (2013).
42. R. Reantragoon *et al.*, Antigen-loaded MR1 tetramers define T cell receptor heterogeneity in mucosal-associated invariant T cells. *J. Exp. Med.* **210**, 2305–2320 (2013).
43. A. J. Corbett *et al.*, T-cell activation by transitory neo-antigens derived from distinct microbial pathways. *Nature* **509**, 361–365 (2014).
44. L. Kjer-Nielsen *et al.*, MR1 presents microbial vitamin B metabolites to MAIT cells. *Nature* **491**, 717–723 (2012).
45. A. N. Keller *et al.*, Drugs and drug-like molecules can modulate the function of mucosal-associated invariant T cells. *Nat. Immunol.* **18**, 402–411 (2017).
46. L. Le Bourhis *et al.*, Antimicrobial activity of mucosal-associated invariant T cells. *Nat. Immunol.* **11**, 701–708 (2010).
47. H.-F. Koay *et al.*, Diverse MR1-restricted T cells in mice and humans. *Nat. Commun.* **10**, 2243 (2019).
48. N. A. Gherardin *et al.*, Diversity of T cells restricted by the MHC class I-related molecule MR1 facilitates differential antigen recognition. *Immunity* **44**, 32–45 (2016).
49. L. Bai *et al.*, The majority of CD1d-sulfatide-specific T cells in human blood use a semi-invariant Vδ1 TCR. *Eur. J. Immunol.* **42**, 2505–2510 (2012).
50. W. Awad *et al.*, The molecular basis underpinning the potency and specificity of MAIT cell antigens. *Nat. Immunol.* **21**, 400–411 (2020).
51. E. J. Adams, Y.-H. Chien, K. C. Garcia, Structure of a γδ T cell receptor in complex with the nonclassical MHC T22. *Science* **308**, 227–231 (2005).
52. L. Wooldridge *et al.*, Tricks with tetramers: How to get the most from multimeric peptide-MHC. *Immunology* **126**, 147–164 (2009).
53. R. Marlin *et al.*, Sensing of cell stress by human γδ TCR-dependent recognition of annexin A2. *Proc. Natl. Acad. Sci. U.S.A.* **114**, 3163–3168 (2017).
54. B. van Wilgenburg *et al.*, MAIT cells contribute to protection against lethal influenza infection in vivo. *Nat. Commun.* **9**, 4706 (2018).
55. M. C. Gold *et al.*, Human mucosal associated invariant T cells detect bacterially infected cells. *PLoS Biol.* **8**, e1000407 (2010).
56. M. D. Crowther *et al.*, Genome-wide CRISPR-Cas9 screening reveals ubiquitous T cell cancer targeting via the monomorphic MHC class I-related protein MR1. *Nat. Immunol.* **21**, 178–185 (2020).
57. W. Awad *et al.*, Atypical TRAV1-2$^-$ T cell receptor recognition of the antigen-presenting molecule MR1. *J. Biol. Chem.* **295**, 14445–14457 (2020).
58. R. W. Birkinshaw *et al.*, αβ T cell antigen receptor recognition of CD1a presenting self lipid ligands. *Nat. Immunol.* **16**, 258–266 (2015).

59. K. S. Wun *et al.*, T cell autoreactivity directed toward CD1c itself rather than toward carried self lipids. *Nat. Immunol.* **19**, 397–406 (2018).
60. S. Huang *et al.*, MR1 uses an endocytic pathway to activate mucosal-associated invariant T cells. *J. Exp. Med.* **205**, 1201–1211 (2008).
61. H. E. G. McWilliam *et al.*, The intracellular pathway for the presentation of vitamin B-related antigens by the antigen-presenting molecule MR1. *Nat. Immunol.* **17**, 531–537 (2016).
62. B. S. Gully, J. Rossjohn, M. S. Davey, Our evolving understanding of the role of the γδ T cell receptor in γδ T cell mediated immunity. *Biochem. Soc. Trans.* **49**, 1985–1995 (2021).
63. G. E. Crooks, G. Hon, J. M. Chandonia, S. E. Brenner, WebLogo: A sequence logo generator. *Genome Res.* **14**, 1188–1190 (2004).
64. J. L. Matsuda *et al.*, Tracking the response of natural killer T cells to a glycolipid antigen using CD1d tetramers. *J. Exp. Med.* **192**, 741–754 (2000).
65. T. M. McPhillips *et al.*, Blu-Ice and the distributed control system: Software for data acquisition and instrument control at macromolecular crystallography beamlines. *J. Synchrotron Radiat.* **9**, 401–406 (2002).
66. M. D. Winn *et al.*, Overview of the CCP4 suite and current developments. *Acta Crystallogr. D Biol. Crystallogr.* **67**, 235–242 (2011).
67. P. D. Adams *et al.*, The Phenix software for automated determination of macromolecular structures. *Methods* **55**, 94–106 (2011).
68. H. Li *et al.*, Structure of the Vδ domain of a human γδ T-cell antigen receptor. *Nature* **391**, 502–506 (1998).
69. P. Emsley, B. Lohkamp, W. G. Scott, K. Cowtan, Features and development of Coot. *Acta Crystallogr. D Biol. Crystallogr.* **66**, 486–501 (2010).
70. W. L. DeLano, The PyMOL Molecular Graphics System. http://www.pymol.org/2/. Accessed 17 November 2021.